

Single crystal growth and superconductivity of $\text{Ca}(\text{Fe}_{1-x}\text{Co}_x)_2\text{As}_2$

Rongwei Hu*, Sheng Ran, Sergey L. Bud'ko, Warren E. Straszheim and Paul C. Canfield
Ames Laboratory, U.S. DOE and Department of Physics and Astronomy, Iowa State University, Ames, IA 50011, USA
(Dated: November 11, 2017)

We report the single crystal growth of $\text{Ca}(\text{Fe}_{1-x}\text{Co}_x)_2\text{As}_2$ ($0 \leq x \leq 0.082$) from Sn flux. The temperature-composition phase diagram is mapped out based on the magnetic susceptibility and electrical transport measurements. Phase diagram of $\text{Ca}(\text{Fe}_{1-x}\text{Co}_x)_2\text{As}_2$ is qualitatively different from those of Sr and Ba, it could be due to both the charge doping and structural tuning effects associated with Co substitution.

PACS numbers: 74.25.Dw, 74.25.F-, 74.62.Bf, 74.70.Xa

The AEFe_2As_2 ($\text{AE} = \text{Ca}, \text{Sr}, \text{Ba}$) of the 122 family is the most extensively studied materials among the various iron arsenic superconductors, since they possess the characteristic tetrahedrally coordinated square planar Fe sublattice, giving rise to lattice instability, antiferromagnetism (AFM) and superconductivity (SC) by chemical substitution, and are readily obtained in large single crystalline form.¹⁻⁶ CaFe_2As_2 is similar to the other two members, it undergoes a phase transition from a high temperature, tetragonal phase to a low temperature, orthorhombic/antiferromagnetic phase below 170 K.⁷ Superconductivity can be induced in CaFe_2As_2 by substituting Fe with Co⁸ or Rh⁹ and As with P¹⁰ and by application of non-hydrostatic pressure^{11,12}, as the tetragonal-orthorhombic/AFM transition is suppressed, strongly suggesting the connection between the AFM fluctuations and SC. However, the physical properties of the single crystals of CaFe_2As_2 are remarkably dependent on the crystal growth procedure. It has been shown that crystals quenched from high temperature using FeAs flux exhibit a transition from a high temperature, tetragonal to a low temperature, non-magnetic, collapsed tetragonal phase below 100 K in contrast to the behavior of CaFe_2As_2 grown from Sn flux.¹³ For Co doping, the as grown, single crystals grown from FeAs-CoAs self-flux, decanted at 1000 °C, do not show any SC as opposed to the corresponding ones grown from Sn flux.¹⁴ Moreover, there is a competing phase of CaFe_4As_3 growing concomitantly with CaFe_2As_2 from Sn flux.⁷ Therefore details in the crystal growth and effects of Co doping in CaFe_2As_2 need to be clarified. In this work, we performed a study of the single crystal growth of $\text{Ca}(\text{Fe}_{1-x}\text{Co}_x)_2\text{As}_2$ out of Sn flux and show the dependence of the magnetic susceptibility and resistivity on Co doping.

Single crystals of $\text{Ca}(\text{Fe}_{1-x}\text{Co}_x)_2\text{As}_2$ were grown from Sn flux in two steps. In order to obtain homogeneous Co substitution for Fe, polycrystalline $\text{Ca}(\text{Fe}_{1-x}\text{Co}_x)_2\text{As}_2$ were prepared first by heating stoichiometric mixtures of Ca, FeAs and CoAs at 900 °C for 24 hours. The polycrystalline sample was ground and pelletized for a second time sintering at 900 °C. Then polycrystalline $\text{Ca}(\text{Fe}_{1-x}\text{Co}_x)_2\text{As}_2$ and Sn with a ratio of 1 : 30 were placed in an alumina crucible and sealed in amorphous silica tubes. The sealed ampoule was heated to 1100 °C and slowly cooled to 600 °C after which the Sn flux

was decanted.¹⁵ This procedure is similar to the one in Ref. 16. Early work on crystal growth of CaFe_2As_2 using Sn flux has identified a needle-shaped orthorhombic phase, CaFe_4As_3 , growing together with CaFe_2As_2 out of Sn flux.⁷ Our crystal growth showed that there was a significant amount of CaFe_4As_3 phase by following the above procedure. For Co doping, the formation of the competing phase may change the composition of the liquid solution, thus it causes complex dependence of the doping concentration of the resulted single crystals on growth conditions. An excess of Ca was added to the polycrystalline and Sn mixture and an optimal $\text{Ca}_{1.5}(\text{Fe}_{1-x}\text{Co}_x)_2\text{As}_2$ was found to be effective for eliminating the CaFe_4As_3 phase. Moreover, there is a solubility problem of $\text{Ca}(\text{Fe}_{1-x}\text{Co}_x)_2\text{As}_2$ in Sn. For the ratio of 1 : 30, in addition to $\text{Ca}(\text{Fe}_{1-x}\text{Co}_x)_2\text{As}_2$ single crystals, there was some undissolved polycrystalline powder after decanting. By changing the ratio to 1 : 45, we were able to completely dissolve the starting polycrystal. The as-grown single crystals were thin plate-like with typical dimension $4 \times 4 \times 0.2 \text{ mm}^3$.

Crystals were characterized by powder x-ray diffraction using a Rigaku Miniflex X-ray diffractometer. The actual chemical composition was determined using wavelength dispersive x-ray spectroscopy (WDS) in a JEOL JXA-8200 electron microscope, by averaging ten spots on the crystal surface. Magnetic susceptibility was measured in a Quantum Design MPMS, SQUID magnetometer. In plane AC resistivity ρ_{ab} was measured by a standard four-probe configuration within MPMS using an LR-700 resistance bridge (frequency = 16 Hz, current = 1 - 3 mA).

Figure 1(a) shows the actual concentration of Co, x_{WDS} , as a function of the nominal $x_{nominal}$, of two series of crystals: using stoichiometric, nominal composition, polycrystalline feedstock, and using polycrystalline feedstock that had 50% excess Ca. The compositional spread of the ten measured spots is taken as the error bar. In contrast to the results in Ref. 16, x_{WDS} deviates from linear dependence on $x_{nominal}$. After the elimination of the competing CaFe_4As_3 phase with 50% excess Ca, x_{WDS} generally increases and has a larger compositional spread, but the curve follows the same trend as the stoichiometric one and the significant non-monotonicity is still present. It is noteworthy that for $x_{nominal}$ greater

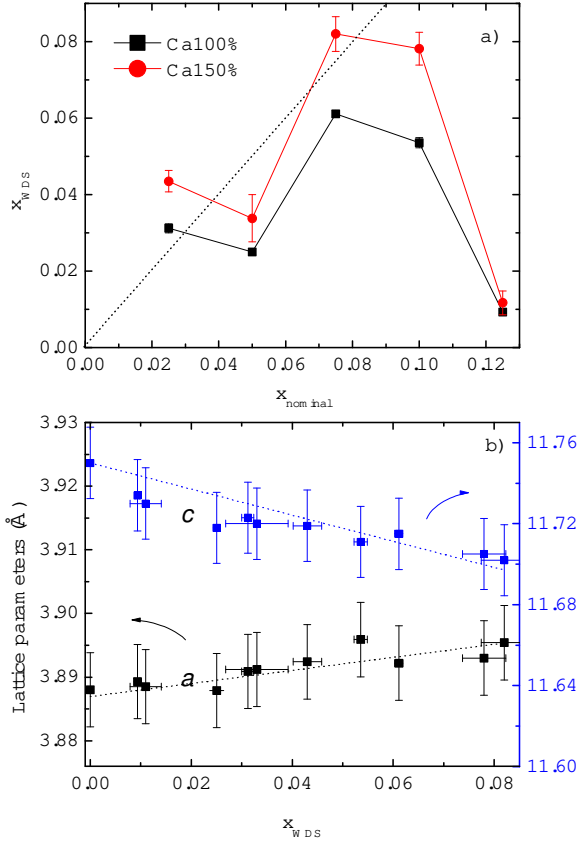


FIG. 1: a) Actual Co concentration as a function of nominal one. Black squares represent the series with stoichiometric starting composition; red circles represent the series with 50% excess Ca in starting composition. Dotted line indicates the ideal slope equal to 1. b) lattice parameters vs. Co doping. Lines are guide to the eye.

that 0.10, the corresponding x_{WDS} decreases dramatically. This behavior suggests difficulties associated with solubility and once again highlights the need to perform WDS measurements on the grown samples. When the lattice parameters (from both series) are plotted as a function of x_{WDS} (Fig. 1(b)), there is a clear linear dependence of a and c parameters on Co-substitution level. The lattice parameters refined by Rietica are shown in Fig. 1(b). Lattice parameter a increases by 0.1% whereas c decreases by 0.4% for $x_{WDS} = 0.082$, similar to the trend in $\text{Sr}(\text{Fe}_{1-x}\text{Co}_x)_2\text{As}_2$. This is also in agreement with the results of Ref. 16, where c linearly decreases, at $x_{EDX} = 0.09$ $\Delta c/c = 0.5\%$, although we do not obtain samples with Co doping higher than 0.08. There are two pairs of concentrations very close to each other by coincidence, i.e. $x_{WDS} = 0.009, 0.011$ and $0.031, 0.033$. Only $x_{WDS} = 0.009$ and 0.031 samples were characterized in the following study.

In-plane magnetic susceptibility of $\text{Ca}(\text{Fe}_{1-x}\text{Co}_x)_2\text{As}_2$

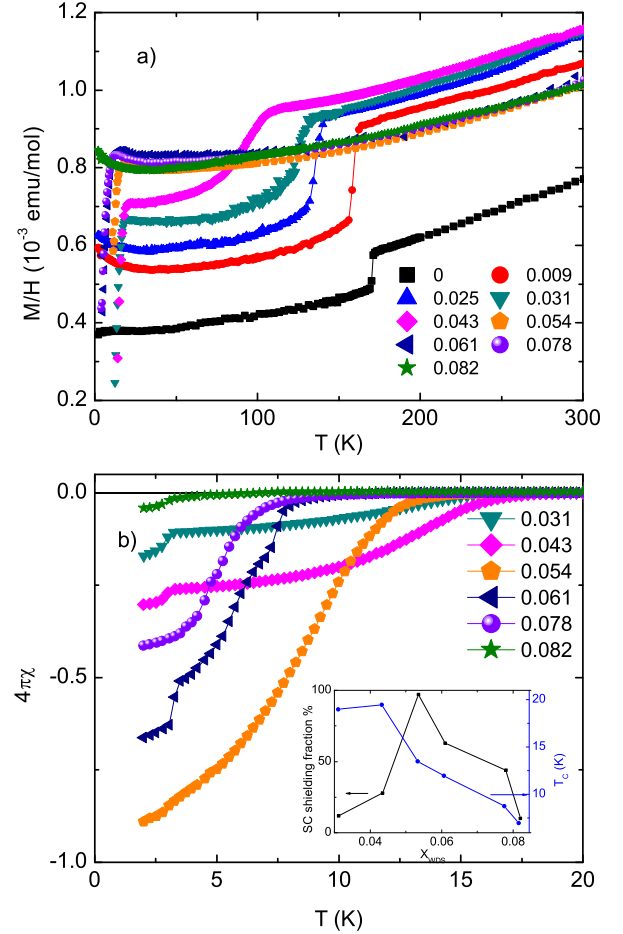


FIG. 2: a) In-plane magnetic susceptibility measured in a magnetic field of 10 kOe as a function of temperature. b) Zero-field-cooled magnetic susceptibility in 50 Oe. Inset shows the variation of superconducting shielding fraction and T_c .

is shown in Fig. 2(a) for magnetic field of 10 kOe. The structural/magnetic transition of the parent CaFe_2As_2 at 170 K is suppressed progressively by Co doping consistent with Ref. 16, until it is completely suppressed at $x = 0.054$. Superconductivity is first detected for $x = 0.031$ and the superconducting transition temperature, T_c , decreases with further substitution. Figure 2(b) shows the zero-field-cooled (ZFC) magnetic susceptibility curves in an applied field of 100 Oe. The small dip at 3.5 K for some curves is due to small Sn flux droplets on the crystal surface. The superconducting shielding fraction, with the contribution from Sn subtracted, varies with doping levels. The highest T_c occurs at $x = 0.043$ whereas the largest volume fraction is reached at $x = 0.054$ with slightly lower T_c (Fig. 2(b) inset). This is similar to what is observed in Ref. 16.

Electrical resistance data, normalized to their room temperature values, are shown in Fig. 3(a) for the Sn flux grown crystals. The anomaly at 170 K for the pure CaFe_2As_2 is suppressed with Co doping, remains sharp until $x_{WDS} = 0.025$ and becomes broad for $x_{WDS} = 0.031$ and 0.043 . (It should be noted that this broadening coincides with the sudden onset of superconductivity.) Figure 3(b) shows the low temperature normalized resistance. The small jump at 3.5 K is due to remanent Sn flux on the crystal. Although $x_{WDS} = 0.031$ shows partial magnetic shielding and its resistance starts to drop at about the same onset temperature, zero resistance is not reached. Complete superconducting transition is observed for $x_{WDS} \geq 0.043$ and T_c gradually decreases with doping in good agreement with the magnetic susceptibility measurements. Nanoscale inhomogeneity and strain due to Co doping may result in wide transitions. But considering the variation and small number of the superconducting volume fraction, SC may not be bulk for many of the $\text{Ca}(\text{Fe}_{1-x}\text{Co}_x)_2\text{As}_2$ samples. Other experimental techniques, e.g. magneto-optical imaging, specific heat, or STM spectroscopy will be required to further clarify the nature/homogeneity of the low temperature state.

Based on the magnetic and transport measurements, $T - x_{WDS}$ phase diagram for $\text{Ca}(\text{Fe}_{1-x}\text{Co}_x)_2\text{As}_2$ is mapped out in Fig. 4(a). The structural and magnetic transitions are inferred from $d\chi/dT$ and $d(\rho/\rho_{300K})/dT$ using the same criteria in Ref. 16. Superconducting transition temperature T_c is inferred from the first deviation from the normal magnetic susceptibility of the ZFC curve. Resistive onset and offset of T_c values are inferred from the intersects of the steepest slope with the normal state and zero resistance respectively. The simultaneous structural and magnetic transition of the pure CaFe_2As_2 is monotonically suppressed by Co doping, but as seen from χ and ρ , the transition remains sharp for low dopings $x_{WDS} \leq 0.025$, no discernible splitting of both transitions can be observed. For $x_{WDS} = 0.031$ and 0.043 , transition broadens and it is possible to infer an upper structural transition and a lower magnetic transition, similar to $\text{Ba}(\text{Fe}_{1-x}\text{Co}_x)_2\text{As}_2$.⁴ To compare the reported phase diagram of $\text{Ca}(\text{Fe}_{1-x}\text{Co}_x)_2\text{As}_2$ in Ref. 16 with ours, we plot the data points (black asterisks) inferred from resistance measurements of Ref. 16 in Fig. 4(a). As can be seen, though our phase diagram shows a faster suppression of the magnetic and structural transitions by Co doping, SC occurs roughly with the same T_c in similar region. It should be noted that the actual Co concentration reaches up to 0.15 in Ref. 16, but only onset of resistive or no superconducting transition is observed above $x = 0.09$, consistent with our observations. We might imagine that an overestimate (underestimate) of the Co concentration in Ref. 16 (our work) will shift the phase diagram.

Different from the superconducting dome in $\text{Sr}(\text{Fe}_{1-x}\text{Co}_x)_2\text{As}_2$ ¹⁷ and $\text{Ba}(\text{Fe}_{1-x}\text{Co}_x)_2\text{As}_2$ ⁴, the onset of SC in $\text{Ca}(\text{Fe}_{1-x}\text{Co}_x)_2\text{As}_2$ appears abruptly at high temperature and gradually decreases with Co

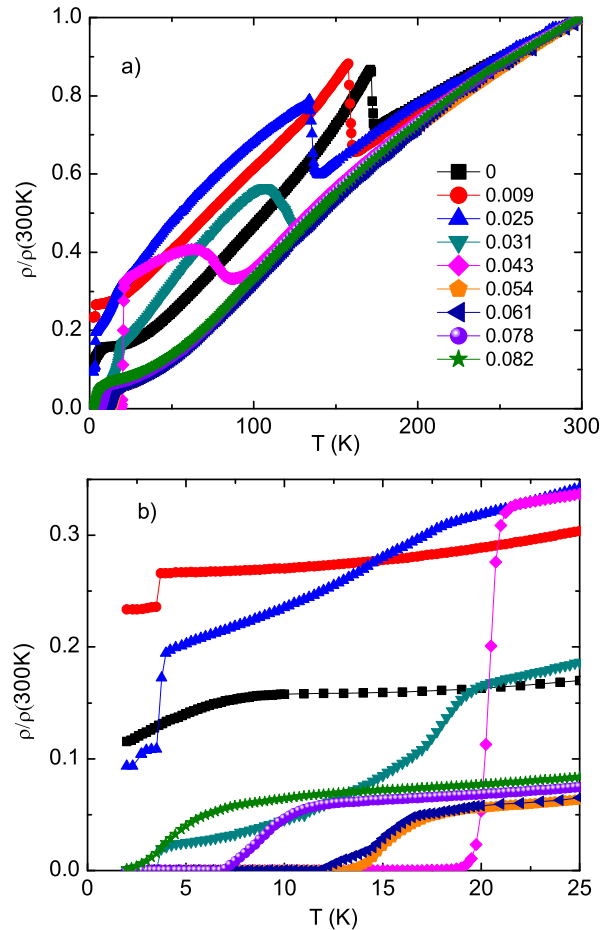


FIG. 3: a) Temperature dependence of the normalized resistivity of $\text{Ca}(\text{Fe}_{1-x}\text{Co}_x)_2\text{As}_2$. b) Expanded view of normalized resistivity at low temperatures.

substitution. In order to compare all three cases of Co doping, the magnetic transition boundaries of Sr and Ba are collapsed on to that of Ca, namely the transition temperatures are normalized by that of the pure parent AEFe_2As_2 and the Co concentrations of Sr and Ba are scaled so as to get to a single manifold in Fig. 4(b). Whereas both the Ba and Sr series manifest a maximum T_c value close to the Co substitution level that drives the magnetic/structural phase transitions to zero, the Ca series manifests maximum T_c values deep in the ordered region and has SC disappearing near the substitution levels needed to suppress the antiferromagnetic/structural phase transition. For the Co substituted Ca122 series the sudden onset of SC may instead be correlated with the splitting of the structural/magnetic phase transition that takes place for $0.025 < x < 0.031$. The reason for this difference is currently not well understood, but may be related to

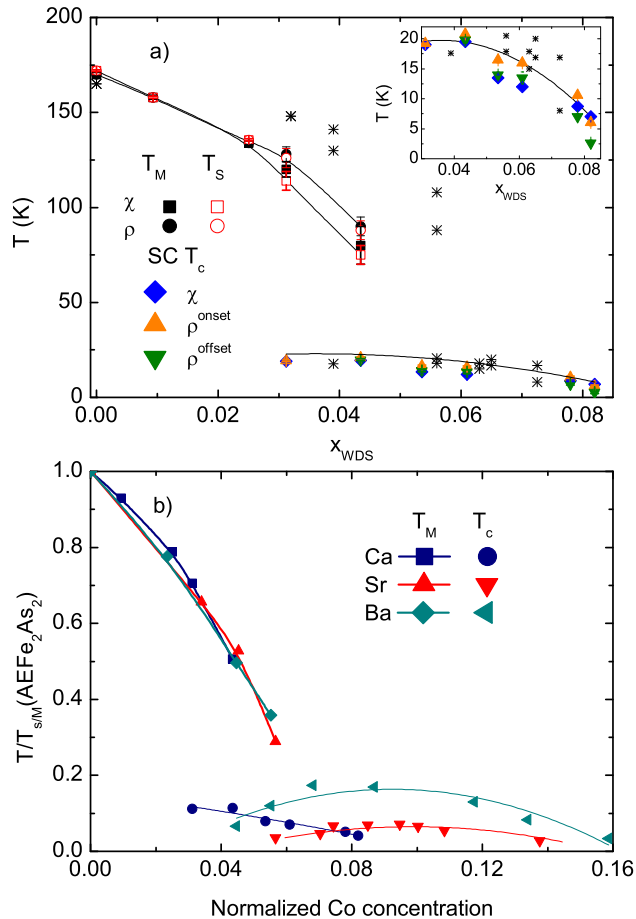


FIG. 4: a) $T - x$ phase diagram of $\text{Ca}(\text{Fe}_{1-x}\text{Co}_x)_2\text{As}_2$. Solid lines are guides to the eye. Inset shows the superconducting region. Black asterisks are the data from Ref. 16 inferred from resistance. b) Comparison of the Ca (this work), Sr^{17} , Ba^4 phase diagrams of Co doping. T_c s are inferred from magnetic susceptibility measurements. Normalization: T axis is normalized by the $T_{S/M}$ of the respective parent compound; (Sr) x axis multiplied by 0.81; (Ba) x axis multiplied by 1.18.

the extreme pressure and strain sensitivity of CaFe_2As_2 as a host material. Unlike Co substituted BaFe_2As_2 or SrFe_2As_2 , it is possible that the changes in lattice parameter seen in Co substituted CaFe_2As_2 play a more important role in determining the phase diagram and represent an additional term to the changes in band filling associated with Co substitution.

In summary, $\text{Ca}(\text{Fe}_{1-x}\text{Co}_x)_2\text{As}_2$ ($0 \leq x \leq 0.082$) have been grown out of Sn flux. We report the details of single crystal growth and their magnetic susceptibility and electrical transport properties. The properties of single crystals are dependent on the growth procedure. The phase diagram of $\text{Ca}(\text{Fe}_{1-x}\text{Co}_x)_2\text{As}_2$ shows a half dome like superconducting region, different from those of $\text{Sr}(\text{Fe}_{1-x}\text{Co}_x)_2\text{As}_2$ and $\text{Ba}(\text{Fe}_{1-x}\text{Co}_x)_2\text{As}_2$. The electron doping as well as chemical pressure probably are both responsible for determining the phase boundary.

This work was carried out at the Iowa State University and supported by the AFOSR-MURI grant #FA9550-09-1-0603 (R. H. and P. C. C.). Part of this work was performed at Ames Laboratory, US DOE, under contract # DE-AC02-07CH 11358 (S. R., S. L. B. and P. C. C.). S. L. Bud'ko also acknowledges partial support from the State of Iowa through Iowa State University.

*Present address: Center for Nanophysics & Advanced Materials and Department of Physics, University of Maryland, College Park MD 20742-4111, USA.

¹ M. Rotter, M. Tegel, D. Johrendt, Phys. Rev. Lett. 101, 107006 (2008).
² Paul C. Canfield and Sergey L. Bud'ko, Annual Review of Condensed Matter Physics, 1, 27 (2010).
³ K. Sasmal, B. Lv, B. Lorenz, A. Guloy, F. Chen, Y. Xue, C.W. Chu, Phys. Rev. Lett. 101, 107007 (2008).
⁴ N. Ni, A. Thaler, J. Q. Yan, A. Kracher, E. Colombier, S. L. Bud'ko, P. C. Canfield, Phys. Rev. B 82, 024519 (2010).
⁵ Deepa Kasinathan, Alim Ormeci, Katrin Koch, Ulrich Burkhardt, Walter Schnelle, Andreas Leithe-Jasper and Helge Rosner, New J. Phys. 11 025023 (2009).
⁶ Yuri Izyumov and Ernst Kurmaev, Springer Series in Ma-

terials Science, 143, 57-107 (2010).
⁷ N. Ni, S. Nandi, A. Kreyssig, A. I. Goldman, E. D. Mun, S. L. Bud'ko, and P. C. Canfield, Phys. Rev. B 78, 014523 (2008).
⁸ Neeraj Kumar, R. Nagalakshmi, R. Kulkarni, P. L. Paulose, A. K. Nigam, S. K. Dhar, and A. Thamizhavel, Phys. Rev. B 79, 012504 (2009).
⁹ Yanpeng Qi, Lei Wang, Zhaoshun Gao, Dongliang Wang, Xianping Zhang, Chunlei Wang, Chao Yao and Yanwei Ma, New J. Phys. 13 033020 (2011).
¹⁰ S. Kasahara, T. Shibauchi, K. Hashimoto, Y. Nakai, H. Ikeda, T. Terashima, and Y. Matsuda, Phys. Rev. B 83,

- 060505(R) (2011).
- ¹¹ P. C. Canfield, S. L. Bud'ko, N. Ni, A. Kreyssig, A. I. Goldman, R. J. McQueeney, M. S. Torikachvili, D. N. Argyriou, G. Luke, and W. Yu, *Physica C* 469, 404 (2009).
- ¹² M. S. Torikachvili, S. L. Bud'ko, N. Ni, and P. C. Canfield, S. T. Hannahs, *Phys. Rev. B* 80, 014521 (2009).
- ¹³ S. Ran, S. L. Bud'ko, D. K. Pratt, A. Kreyssig, M. G. Kim, M. J. Kramer, D. H. Ryan, W. N. Rowan-Weetaluktuk, Y. Furukawa, B. Roy, A. I. Goldman, and P. C. Canfield, *Phys. Rev. B* 83, 144517 (2011).
- ¹⁴ S. Ran, (private communication).
- ¹⁵ P. C. Canfield, *Z. Fisk Phil. Magaz.* B 65, 1117 (1992).
- ¹⁶ L. Harnagea, S. Singh, G. Friemel, N. Leps, D. Bombor, M. Abdel-Hafeez, A. U. B. Wolter, C. Hess, R. Klingeler, G. Behr, S. Wurmehl, and B. Buchner, *Phys. Rev. B* 83, 094523 (2011).
- ¹⁷ Rongwei Hu, Sergey L. Bud'ko, Warren E. Straszheim, Paul C. Canfield, *Phys. Rev. B* 83, 094520 (2011).